Dynamic analysis of an improved shared moorings for floating offshore wind farm

Lu Xie [a], Chun Li [a, b, d], Minnan Yue [a, d], Hongsheng He [a], Wenzhe Jia [a], Qingsong Liu [e], Zifei Xu [c], Li Fan [a], Musa Bashir [c], Yangtian Yan [f]

[a] *School of Energy and Power Engineering, University of Shanghai for Science and Technology, Shanghai, 200093, China*

[b] *Shanghai Key Laboratory of Multiphase Flow and Heat Transfer in Power Engineering, Shanghai, 200093, China*

[c] *Mechanical Engineering and Materials Research Centre (MEMARC), Liverpool John Moores University, Liverpool, Byrom Street, L3 3AF, United Kingdom*

[d] *Non-carbon Energy Conversion and Utilization Institute, Shanghai 200240, China*

[e] *Liverpool Logistics, Offshore and Marine (LOOM) Research Institute, Liverpool John Moores University, Liverpool, Byrom Street, L3 3AF, United Kingdom*

[f] *Faculty of Maritime and Transportation, Ningbo University, Ningbo, 315211, PR China*

Abstract: Shared mooring lines have demonstrated their effectiveness in reducing the installation costs of floating offshore wind farms by minimizing the requirement for multiple anchors. However, this innovation has also brought complex restoring properties and a greater tendency towards resonance. To tackle this challenge, this research presents a novel approach for shared mooring systems, implemented in a 2x2 orthogonal wind farm arrangement featuring 5 MW wind turbines installed on the Barge platform. Through the application of FAST and AQWA, a comparative analysis is conducted juxtaposing the original mooring (OM) and three new mooring models, namely buoy mooring (BM), clump weight mooring (WM) and buoy clump weight mooring (BWM). A comprehensive examination is carried out to assess the impact of on platform and mooring characteristics. The results show that the BM can effectively reduce the platform's surge and sway response, and that the mooring tension and laid length decrease as the net buoyancy increases. The WM increases the response amplitude at the yaw direction. The BWM with link buoys helps to improve the dynamic response of the platform and increases the length of the mooring laid. This analysis provides valuable insights for the design of floating wind farms incorporating shared mooring systems.

Keywords: offshore wind, dynamic analysis, shared-mooring, floating wind turbine

1.Introduction

Wind energy is emerging as a prominent frontrunner in the pursuit of sustainable energy and the mitigation of global carbon emissions by 2030, as outlined in the Paris Agreement (Diesendorf, 2022; IEA, 2021; Summerfield and Park, 2023). In comparison to onshore wind farms, offshore wind farms offer the advantages of high wind speed, stable wind direction, reduced wind shear, enhanced energy density and diminished turbulence intensity (Gaumond et al., 2014). Nevertheless, the conventional fixed support structures utilized in shallow offshore wind turbines encounter notable challenges in adapting to the demanding conditions of deep and remote seas (Lee et al., 2023; Wang et al., 2022). Consequently, the inexorable shift from fixed bases to floating platforms in offshore wind farm development has emerged as an inevitable and compelling trend (Liu et al., 2019; Wang et al., 2019). With increasing of water depths, the mooring system and anchor points for floating wind turbines are on the rise. Hightened mooring cost poses challenges for large-scale development of floating wind farms (Ramachandran et al., 2022). To reduce floating wind farm costs in deep waters, concepts of the shared anchors and shared mooring have been put forth (Fontana et al., 2016; Goldschmidt and Muskulus, 2015). Shared mooring systems incorporate mooring lines that directly connect neighbor platforms, thereby reducing the number of anchors and mooring lines for ultimately enhancing cost-effectiveness. Continuing research endeavors are currently underway to investigate the practical implementation of these approaches.

Ding et al. (2018) proposed Spar platform array floating wind farm and verified the effectiveness of the array wind farm. The results indicated that the shared mooring system effectively improved the surge response of the platform in the wind farm, but increased the sway response of the platform at the edge under severe sea condition. Liu et al. (2021) studied the dynamic response of 3×3 Barge platform array wind farms under extreme sea condition, as shown in the Fig.1. Compared with a single wind turbine, the platform in the array wind farm has better heave, pitch and nacelle stability. Nevertheless, with the increase of wind turbines in the array wind farm, it will exacerbate the surge response of the wind turbine platform in the middle position. Chen ang Yang (2021) compared the experimental and numerical results of semi-submersible platform wind farm. The study verified that the shared moorings effectively reduce the space of wind farms and optimized the shared mooring lines by changing the diameter to improve the stability and minimum breaking load. Lozon et al. (2023) investigated shared moorings and individually moored system wind farms. It was confirmed that the shared moorings increase the equilibrium position and maximum distance of drift in the surge direction. Wilson et al. (2021) employed a linearized model to optimize a variety of shared mooring arrangements. The results demonstrated that the mooring performance can be promoted ideally when the shared mooring is regular polygonal layouts with perpendicular anchor line pairs. However, the mooring weight and return force will increase with the number of wind turbines and the complexity of the arrangement in the wind farm. Liang et al. (2023) researched the Spar platform wind farm with multiple forms of shared moorings, focusing on the effect of wind load and direction on the dynamic response of the platform and mooring tension in the wind farm. The results revealed that the shared mooring on the windward side is subjected to a greater tension than that of a single wind turbine.

The aforementioned investigations demonstrated that shared mooring wind farms reduce the space of wind farms, save costs by reducing the mooring lines and anchors, and improve the dynamic response of the platform in heave, surge and pitch directions. However, it is undeniable that the shared mooring increases the sway dynamic response of platforms. As the shared mooring connects adjacent platforms and is affected by the motion of multiple platforms at the same time, the loads are more complicated and the mooring tension increases compared to the single mooring tension. In order to reduce the mooring tension and improve the mooring performance, some scholars have proposed hybrid mooring (Kwan et al. 2019). Huo et al. (2023) conducted a comparison between a chain and a hybrid mooring system (chain + polymer cable + chain) for shallow offshore wind turbines. The results showed that the hybrid mooring system could effectively reduce platform pitch and heave response and mooring tension. Yan et al. (2018) designed a mooring system with buoys and studied the impact of buoy size and position on the floating platform. The findings indicated that the buoys can reduce the standard deviation of the mooring tension and improve the fatigue life of the mooring.

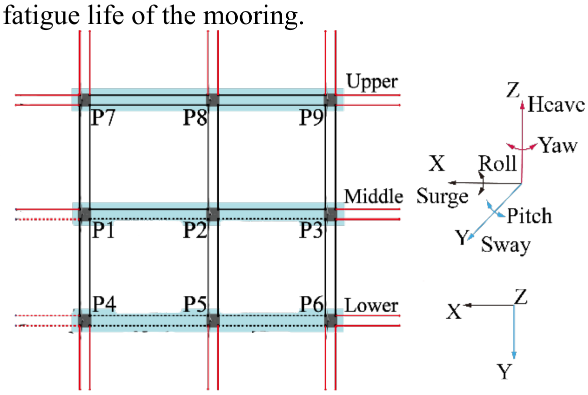

Fig.1 The top view of mooring system of barge platforms in wind farm

Motivated by the concept of hybrid mooring, the application of hybrid mooring to shared mooring systems has been explored for the purpose of enhancing their performance. The concept of utilizing hybrid mooring has been proposed in the context of floating offshore wind turbines, with the objective of mitigating excessive tension in shared mooring systems and reducing the risk of fatigue damage. However, unlike traditional offshore platforms, the underlying mechanical interactions between wave-flow coupling and hybrid mooring remain unclear.

Therefore, this study employs a 5 MW wind turbine as the baseline model and establishes a coupled dynamic model of a 2x2 array barge-based floating wind farm equipped with a shared hybrid mooring system, utilizing AQWA and FAST. By investigating the dynamic responses and mooring characteristics of wind turbines under the combined influence of wind and waves, the effectiveness of hybrid mooring in reducing mooring loads for floating wind farms is demonstrated. Furthermore, an analysis of buoy and clump weight parameters, along with their positions within the shared mooring system, is conducted to evaluate their impact on the dynamic response and stability of the floating wind farm. This analysis provides theoretical support for the design of shared mooring systems in floating offshore wind farms.

The remainder of the paper is structured as follows: Section 2 presents a 2 x 2 array wind farm based on the 5MW Barge platform wind turbine and describes three hybrid mooring models. Section 3 refers to the dynamic equations governing the motion and environmental loads. Section 4 verifies the reliability of wind farm models by comparing the numerical results of the Spar platform with the experimental values. Section 5 compares and analyses the effects of three mooring systems on the platform's natural frequency, dynamic response, mooring tension and laid length. Finally, the study concludes with a summary of findings in Section 6.

2. Wind farm and mooring system model

In this section, a 2 × 2 array wind farm and a hybrid mooring model based on the 5 MW Barge platform wind turbine are introduced.

2.1 2 × 2 Barge wind farm

The Barge platform is known for its simplicity, easy positioning, and cost-effectiveness. However, it has a shallow draft and a high center of gravity, making it more susceptible to wind and wave excitations and prone to deflection (Wayman, 2006). Previous studies have shown that arrayed wind farms can effectively improve the dynamic response of platforms compared to single platforms.

Table 1 and Table 2 present the main parameters of the 5 MW wind turbine and the Barge platform (Jonkman et al., 2009). To minimize the influence of wind turbine wake in the wind farm, the spacing between horizontal axis wind turbines is set to 7 D-8 D between the front and back (Choi et al., 2013), 3 D-5 D between the left and right (Stevens et al., 2014), where D presents the Rotor diameter of wind turbines. Based on these considerations, a 2 × 2 Barge platform wind farm consisting of four wind turbines is constructed with an adjacent distance of 700 m. In order to investigate better the impact of wind and waves on wind farms, this paper simulates the situation when the wind and the waves are at an angle of 180°. (Fig.2).

Table.1

Parameters of NREL 5 MW wind turbine

Parameter	Value	Parameter	Value
Rating power/MW	5	Rotor diameter/m	126
Blades	3	Cut-in wind speed /m·s^{-1}	3
rated speed /rpm	12.1	Cut-out wind speed /m·s^{-1}	25
Rated wind speed /m·s^{-1}	11.4	Hub height /m	90
Hub diameter /m	3	Tower mass /kg	3.5×10^5
Rotor mass /kg	1.1×10^5	Nacelle mass /kg	2.4×10^5

Table.2

Platform parameters of ITI Barge

Parameter	Value	Parameter	Value
Length × width /m	40×40	Mass center /m	-0.282
Draft /m	4	Roll inertia /kg·m^2	7.269×10^8
Water displacement /m^3	6000	Pitch inertia /kg·m^2	7.269×10^8
Total mass of platform /kg	5.452×10^6	Yaw inertia /kg·m^2	1.454×10^9

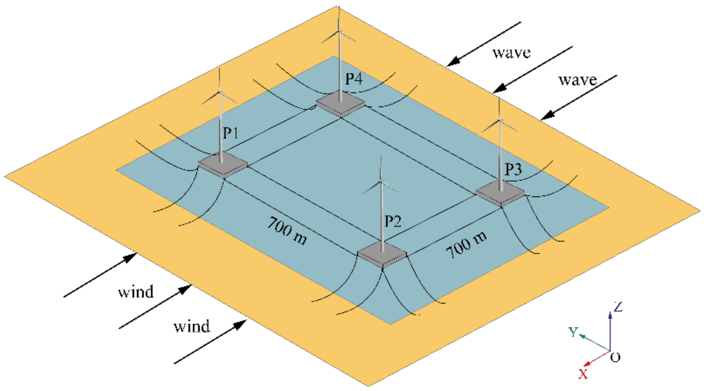

Fig.2 2×2 Barge array wind field

2.2 Mooring system

In wind farms, there are two main types of moorings: fixed moorings and linked moorings (Jonkman and Matha, 2010). The Moorings are made by chain. The key parameters of these moorings are presented in Table.3.

Table.3

2×2 Array Barge platform floating wind farm mooring system parameters

Parameter	Link catenary	Fixed catenary
Mass/(kg/m)	120	250
Equivalent diameter/m	0.05	0.16
Maximum tension/N	7500000	7500000
Axial stiffness/(N/m)	589000000	589000000
Length/m	680	480

To improve the platform stability, three hybrid mooring configurations are proposed on the basis of the array shared mooring: buoy mooring (BM), clump weight mooring (WM) and buoy-clump weight mooring (BWM). Synthesis of the extensive previous research，the specific parameters for the buoy and clump weight components are presented in Table 4 (Mavrakos and Chatjigeorgiou, 1997), and the arrangement can be observed in Fig.3. In this draw, the fixed mooring links the platform to the seabed, and the linked mooring connects the two platforms.

Table.4
Buoy and clump weight parameters

Parameter	Clump weight range	Link buoys	Fixed buoys
Mass/t	2 - 20	12	15
Additional mass factor	0.425	1	1
Additional damping factor	0.125	1.2	1.2

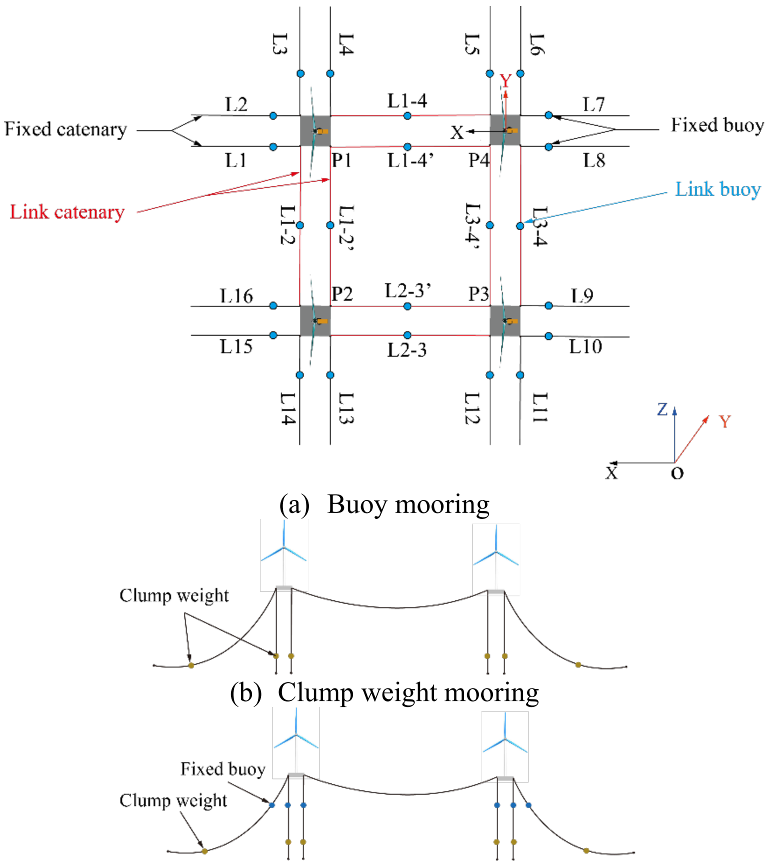

(c) Buoy - clump weight mooring

Fig.3 Diagram of wind farm with different mooring systems

The commonly used method for a fully coupled model of a floating wind turbine moorings is the quasi-static method (Ma et al., 2014; Karimirad, 2013; Jeon et al., 2013). This means that the moorings are in quasi-static equilibrium at any given moment. Nevertheless, the dynamic effects from the platform motions may not be accurately evaluated. Hall et al. (2011, 2015) verified the reliability of the dynamic modelling approach by comparing it with experimental results of a semi-submersible floating wind turbine. To accurately calculate the mooring dynamics, the finite element method was used to model the mooring as a chain of Morison units subjected to external forces, as shown in Fig.4.

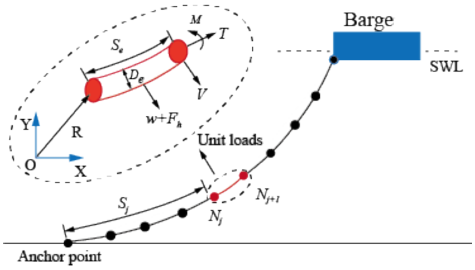

Fig.4 The dynamic model of a mooring line

The equations of motion for an arbitrary unit of moorings are as follows (Ansys, 2013):

$$\begin{cases} \partial T / \partial S_\mathrm{e} + \partial V / \partial S_\mathrm{e} + w + F_\mathrm{h} = m_\mathrm{e} \cdot \partial^2 R / \partial t^2 \\ \partial M / \partial S_\mathrm{e} + \partial R / \partial S_\mathrm{e} \cdot V = -q \end{cases} \quad (1)$$

where T and V are the tension and shear vectors at the first node of the unit respectively; S_e is the unstretched length of the element; De is the diameter of the element; w and F_h are the weight of unit length and hydrodynamic load vectors; m_e is the unit length structural mass; R is the position vector at the first node of the unit; and M is the bending moment vector at the first node of the unit; q is the distributed moment loading per unit length.

Mooring bending moments and tensions are calculated as follows:

$$\begin{cases} M = EI \cdot \partial R / \partial S_\mathrm{e} \cdot \partial^2 R / \partial S_\mathrm{e}^2 \\ T = EA \cdot \varepsilon \end{cases} \quad (2)$$

where EI and EA are the bending stiffness and axial stiffness of the mooring respectively; ε is the axial strain of the mooring.

For the added buoys and clump weight mooring unit, F_h contains the drag force load (F_d), the buoyancy load (F_b) and the radiation load associated with the added mass. For the added float counterweight mooring unit with an added mass matrix of m_a, the hydrodynamic load F_h is calculated as in equation (3):

$$F_\mathrm{h} = F_\mathrm{b} + F_\mathrm{d} - m_\mathrm{a} [\vec{a}_j, \vec{a}_{j+1}]^\mathrm{T} \quad (3)$$

where $\vec{a}_j$ is the acceleration of the mooring at node j.

3. Environmental loads

In complex marine environments, floating wind turbines experience multiple environmental loads, including wind and waves, as well as the constraints imposed by their mooring system. The motion control equation of a floating wind turbine can be expressed as below (Cummins et al., 1962).

$$\{m + A_\infty\} \ddot{X}(t) + D\dot{X}(t) + KX(t) + \int_0^t R(t-\tau)\dot{X}(\tau)d\tau = F_\mathrm{wind}(t) + F_\mathrm{w}(t) + F_\mathrm{m}(t) \quad (4)$$

where m and A_∞ are structure mass and added mass; D and K are damping and hydrostatic stiffness; $\ddot{X}(t)$, $\dot{X}(t)$ and $X(t)$ are the system acceleration matrix; the system velocity matrix and the system displacement matrix; $R(t-\tau)$ is a delay function; F_wind, F_w and F_m is wind load, wave load and mooring load.

3.1 Hydrodynamic model

The Morison equation and the potential flow theory are the main methods employed to calculate wave forces on floating platforms. The potential flow theory is commonly used in AQWA, where the fluid is assumed as a spinless, inviscid, incompressible flow with the following boundary conditions: impermeable seabed, free liquid surface, free surface and impermeable floating body surface. The velocity potential function Φ is obtained from the Laplace equation, expressed as (Newman, 1979):

$$\Phi = \Phi_I + \Phi_D + \Phi_R \quad (5)$$

$$\partial^2 \Phi / \partial x^2 + \partial^2 \Phi / \partial y^2 + \partial^2 \Phi / \partial z^2 = 0 \quad (6)$$

$$\partial \Phi / \partial z = 0 \quad (7)$$

$$g \partial \Phi / \partial z + \partial^2 \Phi / \partial t^2 = 0 \quad (8)$$

$$\partial \Phi / \partial z = \partial \eta / \partial t + (\partial \eta / \partial x) \cdot (\partial \Phi / \partial x) + (\partial \eta / \partial y) \cdot (\partial \Phi / \partial y) \quad (9)$$

$$\partial \Phi / \partial \vec{n} = 0 \quad (10)$$

where Φ_I is the incident potential; Φ_D is diffraction potential; Φ_R is the radiation potential; g is the acceleration of gravity ; η is the volume fractions of water and air; $\vec{n}$ is the surface normal vector of marine structure. The Bernoulli equation gives the hydrodynamic pressure on the surface of the floating body and the wave load and wave vector are solved as follows, where S_B is the wet surface:

$$p = -\rho \partial\Phi / \partial t \tag{11}$$

$$F_w = \iint_{S_B} -p\vec{n} \mathrm{d}S_B \tag{12}$$

$$M_w = \iint_{S_B} -p(\vec{r} \times \vec{n}) \mathrm{d}S_B \tag{13}$$

In this study, the hydrodynamic calculation software AQWA is utilized to generate irregular waves using the Pierson-Moskowitz spectrum (P-M spectrum) (Pierson and Moskowitz, 1964). The P-M spectra is derived from actual data in the North Atlantic and is suitable for the analysis of marine structures in growth or full developmental stages. The selected wave parameters are a significant wave height of 3.2 m and a zero-crossing period of 10 s. Figure 5 depicts the frequency domain of the generated wave.

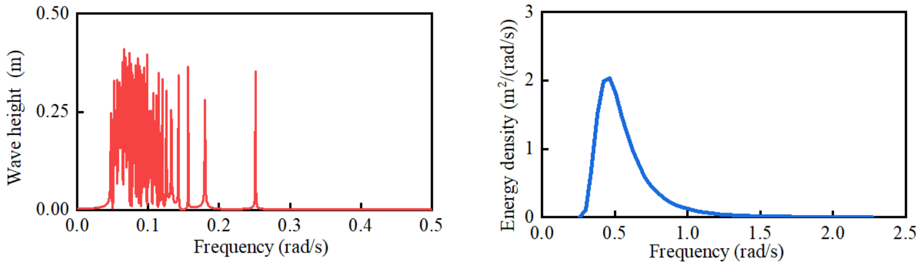

Fig.5 Wave frequency domain

3.2 Aerodynamic model

The Blade element momentum theory (BEM) is used to calculate the aerodynamic load in FAST V8 (Moriarty and Hansen, 2010). The wind load is solved by decomposing the blade into n segments along the wingspan direction, as illustrated in Fig.6. Where V is the incoming wind speed; Ω is the rotational angular velocity; α_i is the angle of attack; β_i is the pitch angle; a is the axial induction factor; b is the tangential induction factor. Integrating the aerodynamic forces of each blade element to obtain the whole blade force. The lift force dL, drag force dD, thrust force dT and torque dM on the blade element unit are calculated as follows:

$$dD = 0.5 C_l \rho c W^2 \mathrm{d}r \tag{14}$$

$$dL = 0.5 C_d \rho c W^2 \mathrm{d}r \tag{15}$$

$$\mathrm{d}T = 0.5 \rho W^2 c (C_l \cos\varphi + C_d \sin\varphi) \mathrm{d}r \tag{16}$$

$$\mathrm{d}M = 0.5 \rho W^2 c (C_l \sin\varphi - C_d \cos\varphi) r \mathrm{d}r \tag{17}$$

where ρ is the air density; W is the relative wind speed at r from the blade root; c is the chord length; φ is the angle of entry; C_l and C_d are the lift and drag coefficients of the cross-sectional airfoil respectively.

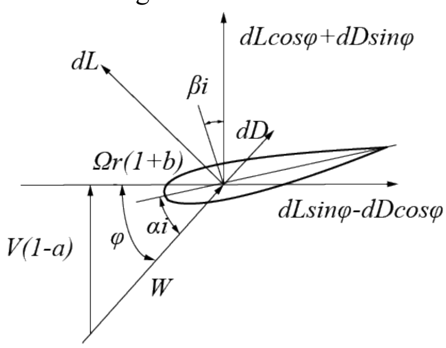

Fig.6 Blade element unit velocity triangle

In this paper, the aerodynamic load consists of two components: the wind turbine rotor rotation generated by the thrust generated by the rotation of the wind turbine rotor, and the wind resistance of the tower and platform structures above the water surface relative to the wind direction. Floating wind turbines are always in dynamic motion, and in order to accurately calculate the effect of aerodynamic loads on their dynamic response, the wind turbine thrusts calculated in FAST V8 were exported and compiled into an AQWA 2019-recognizable external file for computation. The dynamic response of the platform under wind and wave loading was investigated.

4. Validation

A validation of the AQWA model for single Spar was preformed to verify the accuracy and reliability of the hydrodynamic calculation model before going into the actual investigation about the dynamic response of single Barge and Barge array.

In case of experimental study for single Spar which was conducted by the Korea Ocean Research and Development Institute (Kord, 2012), used for the AQWA model validation (the full-scale water depth is about 144m and the scale ratio is 45:1. Besides, waves used in the experiment are regular waves under head sea conditions and the wave frequency range is from 0.1 to 1.5 rad/s), as well as those used for the preliminary assessment of the single Barge.

For AQWA, mesh generation is mainly based on the following principles. The area ratio of adjacent grid cells should not exceed 3. Besides, characteristic dimensions of every grid cell should be less than 1/7th of the incident wavelength (Ding et al., 2018). Furthermore, for 32-bit version of AQWA solver number of the panels is limited to 18000, of which 12000 may be diffracting, while the 64-bite version of AQWA solver is limited to 40000, of which 32000 may be diffracting. The smaller the maximum panel size, the more accurate the results would be, yet more calculation resources would be needed. According to the mentioned principles above, mesh generation work was conducted with the maximum size of 1.2m, while the diffraction panel under the waterline is 1m and the Morison element is 0.5m. Results of the mesh generation are shown in Fig.7. Total number of panels is about 16000, of which number of diffraction panels is about 8000 and Morison elements are 120.

Fig.7 Mesh distribution of single Spar

The surge, heave and pitch RAO in frequency-domain can be seen in Fig.8. As can be seen in Fig.8, surge response amplitude operator (RAO) shows the trend of decrease with the increase of wave frequency, while the heave and pitch RAO show the trend of first increase and then decrease. Peak wave frequency of heave RAO is about 0.2rad/s, while it's about 0.22rad/s for pitch RAO. Although there exist slight differences for surge and pitch RAO compared with the experimental studies, it could still be thought that the simulation results show quite good agreements with the KORDI experimental results because of the effect of viscous damping as well as test errors.

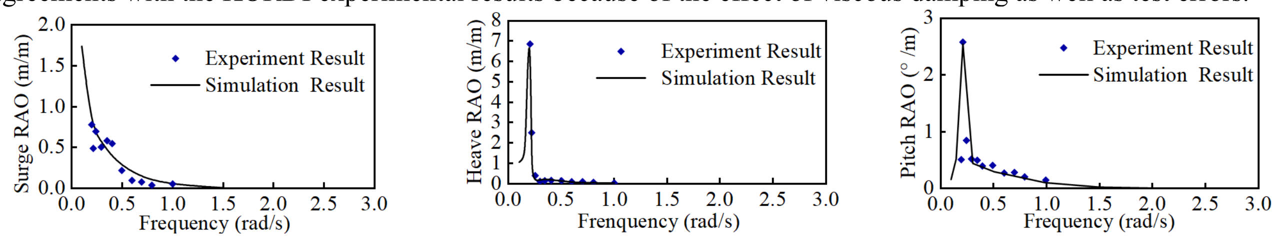

(a) Surge (b) Heave (c) Pitch

Fig.8 RAO in frequency domain of original Spar

Therefore, we used same mesh generation strategy in single barge, the diffraction unit under the waterplane is refined. The maximum unit size of the barge platform is 1.5 m, the total number of diffraction units is about 3000, and the non-diffracting units is about 5000. The result of the mesh generation is shown in Fig.9.

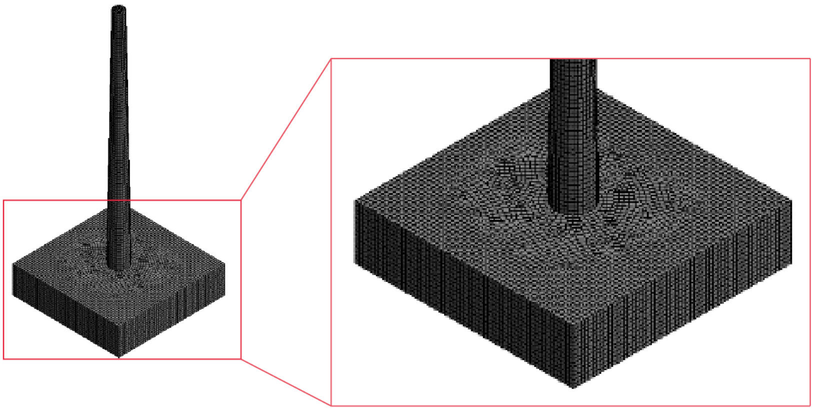

Fig.9 Mesh generation of floating wind turbine on Barge platform

In order to verify the reliability of the hydrodynamic model used in this study. AQWA hydrodynamic calculations were employed to determine the second-order average drift force in surge using both the far-field method and the near-field method. The results obtained from both methods exhibited similar trends and orders of magnitude. Figure 10 presents the results of these calculations. Therefore, it can be concluded that the current grid division satisfies the hydrodynamic calculation requirements.

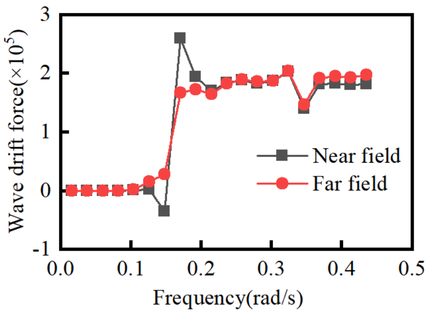

Fig. 10 Barge platform second order mean drift force in surge

5. Result and discussion

This section investigates the impact of BM, WM and BWM on platform motion, mooring tension and mooring laid length in a wind field with varying wind and wave directions at a depth of 150 m. The net buoyancy of the buoys is selected within the range of 0.2 G to 0.6 G (G indicates the mooring weight of the overhanging section) based on empirical values from Mavrakos et al. (1991). The buoy positions are varied between 50 m and 200 m from the fairlead. The weight of the clump weight is 2 t, 5 t, 10 t, 15 t, and 20 t, and its position varies between 100 m and 350 m from the fairlead. Furthermore, two different BWM arrangements are considered, one with link buoys and one without. The Kaimal wind spectrum model (Jonkman and Kilcher, 2012), and the Pierson-Moskowitz (P-M) wave spectrum are employed to simulate the wind and waves in the environment. The main environmental parameters are provided in Table 5 (Johannessen et al., 2002). Under the combined influence of the wind and waves, the floating platform experiences six degrees of freedom (6 DOF) motion, namely surge, sway, heave, pitch, roll and yaw, as illustrated in Fig.11.

Table.5
Environmental parameters

Parameters	Values
Mean wind speed /m·s^{-1}	11.4
Turbulence intensity	0.14
Significant wave height /m	3.2
Zero-crossing period /s	10
Current/m·s^{-1}	0.8

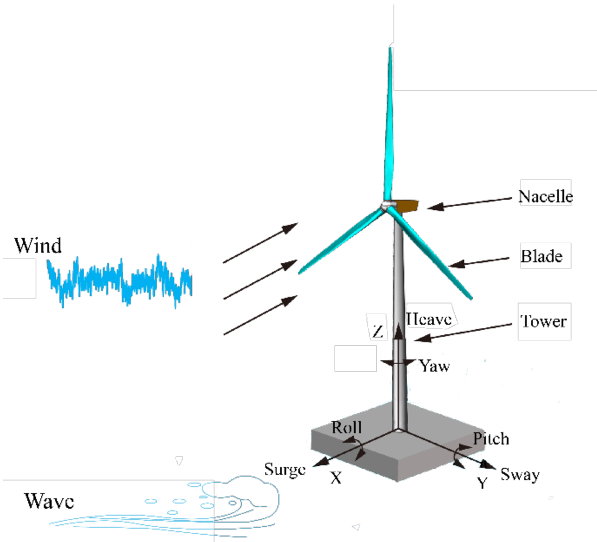

Fig.11 Platform degrees of freedom

5.1 Platform frequency domain analysis

The natural frequencies of platforms 1 (P1) and 4 (P4) in the wind farm are analyzed to examine the impact of buoys and clump weights. The Fourier transform of the free decaying motion of the platforms in 6 DOF is utilized to determine their respective natural frequencies. The natural frequencies of P1 and P4 are presented in Fig.12 and 13, respectively.

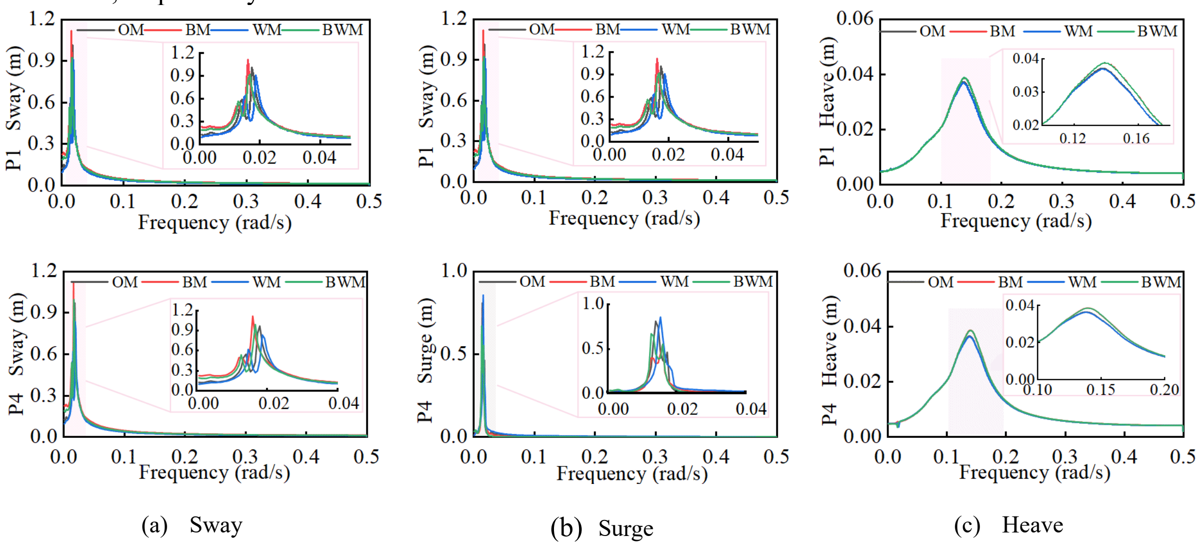

Fig.12 Natural frequency in the direction of platform translation

Fig.12 illustrates the natural frequencies of the platform in the sway, surge, and heave directions. The sway and surge natural frequencies are concentrated around 0.02 rad/s, while the heave natural frequency is 0.14 rad/s. The addition of buoys has a minimal impact on the heave natural frequency but affects the sway and surge natural frequencies to some extent. Specifically, the BM system reduces the natural frequency of the platform in the sway and surge directions, while the WM system increases it in both directions. However, the BWM system has the same effect as the BM system on the sway and surge natural frequencies. Therefore, it is considered that the buoy has a greater influence on the natural frequency of the platform compared to the clump weight. In terms of response amplitude, the BM system increases the response amplitude in the surge, sway and heave directions of P1, but decreases the response amplitude at the surge frequency of P4. By contrast, the WM system reduces the response amplitude of the platform in all directions except for heave and surge of P4.

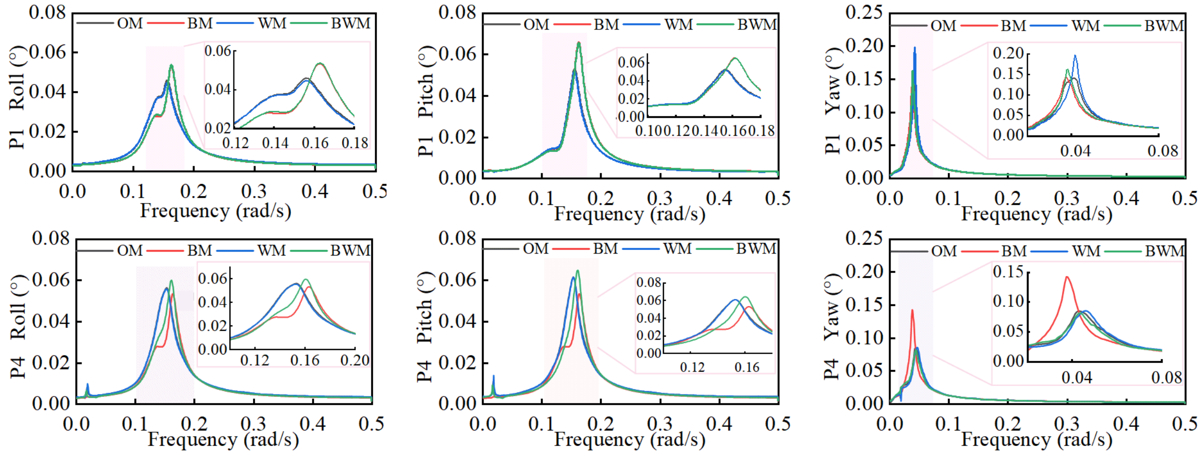

(a) Roll (b) Pitch (c) Yaw

Fig.13 Natural frequency in the direction of platform rotation

As shown in Fig.13, the natural frequencies of the platform in the roll, pitch and yaw directions are concentrated around 0.14~0.17 rad/s and 0~0.06 rad/s respectively. The WM system does not change the natural frequencies and amplitudes of the platform in the roll and pitch directions, showing a consistent trend with the original mooring (OM) system. On the other hand, both the BM and BWM system increase the natural frequency of the platform in the roll and pitch directions. The WM system increases the response amplitude at the natural frequency of the yaw response for P1 but does not modify the natural frequency itself. This indicates that the WM system mainly functions on the amplitude of the natural frequency in the yaw direction, while the natural frequency and amplitude in the direction of pitch and roll are mainly influenced by the buoys. In summary, it can be concluded that the BM system will increase the response amplitude in all directions except for the yaw response, while the response amplitude in the yaw direction is mainly influenced by the clump weights. The buoys have an impact on the natural frequency of the platform in the sway, surge, roll and pitch directions in some degree, but they do not affect the natural frequency in the heave direction.

5.2 Platform dynamic response

This section explores the impact of the BM, WM and BWM system on the platform motion. To account for the symmetry of Barge platform and wind field arrangement, P1 and P4 are chosen as the primary subjects of investigation. The aim is to examine the variations in dynamic response of platforms under different wind and wave conditions, utilizing a simulation duration of 1800 seconds.

5.2.1 Buoy mooring system

As the dynamic response of heave, roll and pitch is not significantly influenced by variations in buoy position, these results are not included in this section. Instead, the time domain curves of surge, sway, and yaw are presented in Fig.14.

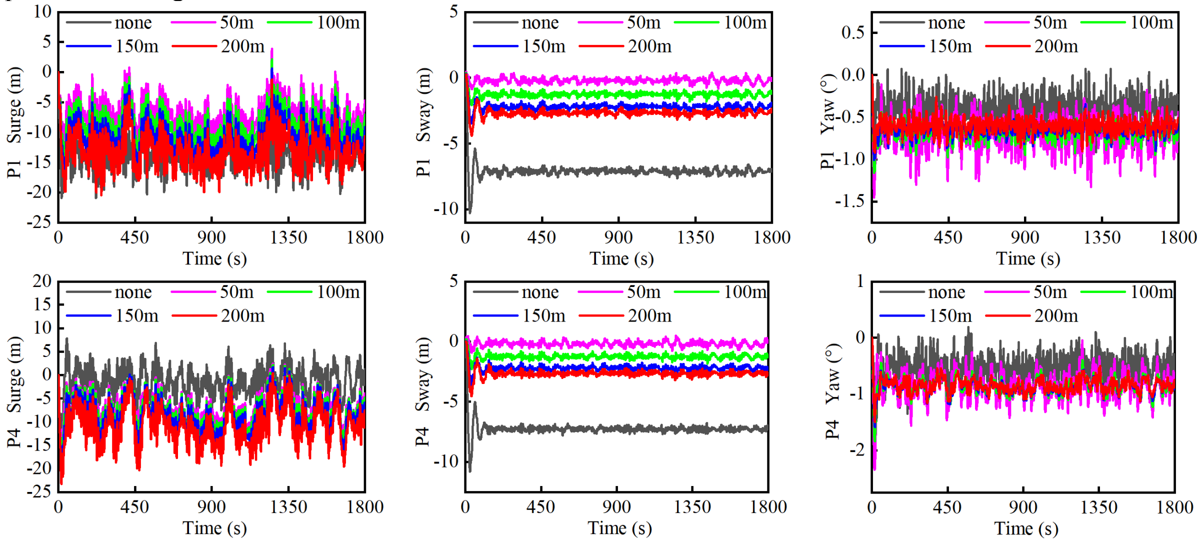

(a) Surge (b) Sway (c) Yaw

Fig.14 Dynamic response of the platform at different buoys positions

It can be noted from the Fig.14 that the surge displacement of platforms P1 and P4 increases with an increase in the distance between the buoy and the fairlead. The surge displacement of P1 is the largest when no buoy is added and decreases as the buoy distance decreases to 50 m. However, for P4, the surge displacement is lowest when no buoy is added and increases with the distance between the buoy and the fairlead increases. In the sway direction, both P1 and P4 exhibit a similar trend. The sway displacement of the platform gradually increases as the distance between the buoy and the fairlead increases, but the sway response of the platform significantly decreases compared to the platform without buoys. In the yaw direction, the response amplitude initially increases when the buoys are added at a distance of 50 m. However, when the distance exceeds 50 m, the response amplitude in this direction is effectively reduced and the stability in the yaw direction is improved. The addition of buoys greatly reduces the sway response of the platform, with a more significant reduction observed as the distance decreases. Nevertheless, with regard to surge response, the behavior of the platform differs depending on the wind and wave sides. On the windward side of P1, the buoys are positioned closer to the platform to minimize the surge response. Conversely, on the leeward side of P4, the buoys actually increase the surge displacement of the platform. To further investigate this phenomenon, a Fourier transformation of the time-domain curve depicting the dynamic response of P4 was performed to obtain the frequency domain representation, as illustrated in Fig.15.

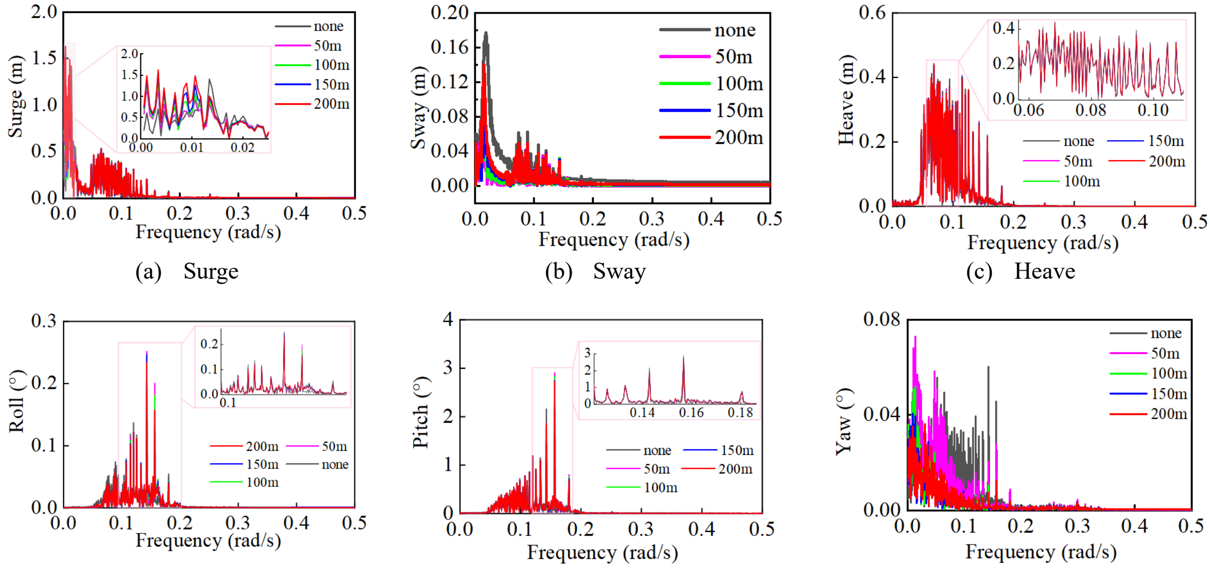

(a) Surge (b) Sway (c) Heave

(d) Roll (e) Pitch (f) Yaw

Fig.15 Frequency domain response of P4 at different buoys positions

By comparing the wave frequency domain, the natural frequency and frequency domain response curves of P4, it is observed that there are two peak ranges of platform surge and sway response frequencies, respectively in 0~0.02 rad/s and 0.05~0.15 rad/s. The former is primarily influenced by the natural frequency in the surge and sway direction, while the latter aligns with the wave frequency range and is mainly affected by the wave frequency. The heave response frequency is predominantly concentrated in the range of 0.05~0.15 rad/s, with a stronger influence from the wave frequency. The roll and pitch response frequencies mainly fall within the 0.05~0.15 rad/s range, influenced by both the wave frequency and platform's natural frequency. Whereas, the peak frequency is controlled by the platform natural frequency. The yaw response frequency mainly focuses on 0~0.15 rad/s, which is affected by both wave frequency and natural frequency. Around 0~0.05 rad/s, which corresponds to the natural frequency of yaw motion, the addition of buoys increases the response amplitude. The range of 0.05~0.15 rad/s primarily represents the wave frequency range, and the addition of buoys reduces the response amplitude at the wave frequency. In addition, changing the distance of the buoy from the fairlead does not impact the frequency of the platform's response but impacts the amplitude of the response. Furthermore, the surge response is greatly influenced by the wave frequency. Adding buoys does not alter the response amplitude at the wave frequency in the surge direction, indicating that increasing the number of buoys does not improve the surge response of P4 on the wave side. Conversely, buoys have the ability to reduce the response amplitude at the natural frequency and wave frequency in the sway direction, resulting in an overall improvement in the sway response of the platform. Moreover, the response amplitude at the natural frequency of yaw motion is influenced by the distance of the buoys, with the response amplitude decreasing as the distance between the buoys and the fairlead increases. Additionally, buoys significantly reduce the response amplitude at wave frequencies.

In spite of buoy distance, the net buoyancy of the buoys also plays a significant role in influencing the dynamic response of the wind farm platform. The response of the platform in surge, sway, and yaw directions, considering different net buoyancies of the buoys, is depicted in Fig.16.

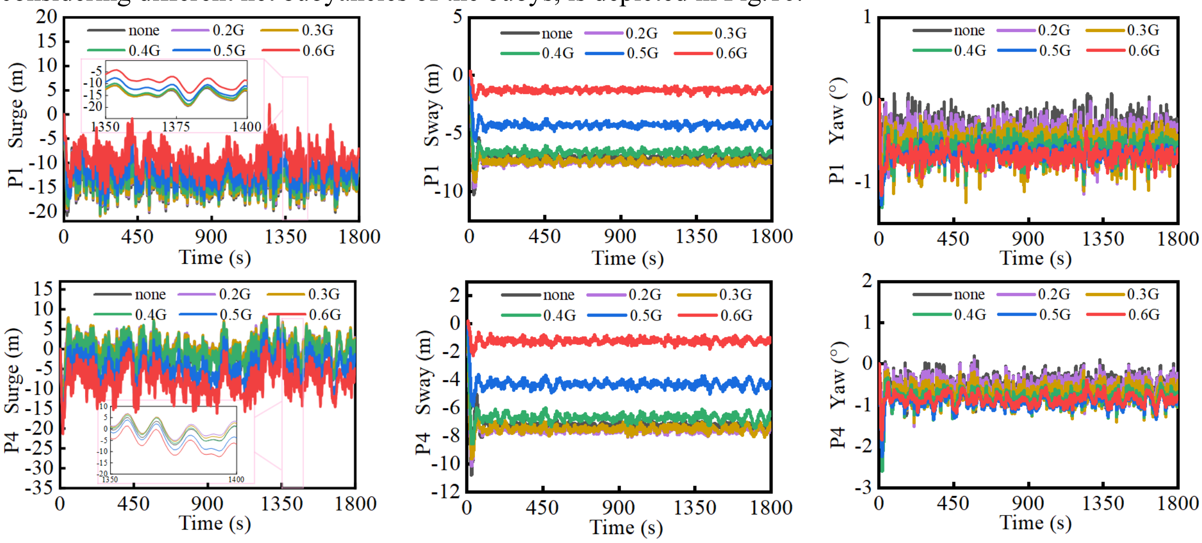

(a) Surge (b) Sway (c) Yaw

Fig.16 Dynamic response of the platform at different net buoyancy

According to the numerical simulation, the buoys mainly affect the dynamic response of the platform in the surge, sway and yaw directions, while their impact on the remaining dynamic responses is minimal. Therefore, the analysis primarily focuses on the response of the platform in these three directions. The main phenomenon is as follows: Firstly, in the sway direction, when the net buoyancy of the buoys is below 0.4 G, it has a negligible effect on the sway response. Nevertheless, when the net buoyancy exceeds 0.4 G, the drift of the platform in the sway direction decreases significantly as the net buoyancy increases. Secondly, in the surge direction, the amplitude of the surge response of P1 decreases with increasing net buoyancy. On the other hand, the drift distance of P4 in the surge direction increases with net buoyancy. The dynamic response of the platform in the sway and surge directions is influenced by the mooring damping. The buoy increases the mooring damping resulting in a reduction in platform drift in the sway and surge directions. Finally, in the yaw direction, the increasing net buoyancy reduces the vertical restraint force of the platform. This, in turn, exacerbates the response in the yaw direction.

5.2.2 Clump weight mooting system

The analysis of the platform's natural frequencies in the WM system indicates that it has minimal impact on the natural frequencies and response amplitudes in the surge and sway directions. Furthermore, it does not significantly alter the frequencies and amplitudes in other response directions. To further research the effect of the weight and position, the specific calculation cases are presented in Table 6 by controlling for one of these factors to examine the influence of the other, and the numerical calculation results are illustrated in Fig.17 and Fig.18.

Table.6
Calculation cases settings

Cases	Weight	Distance from fairlead	Cases	Distance from fairlead	Weight
C1	2 t	100 m	C1’	350 m	2 t
C2		150 m	C2’		5 t
C3		200 m	C3’		10 t
C4		250 m	C4’		15 t
C5		300 m	C5’		20 t
C6		350 m			

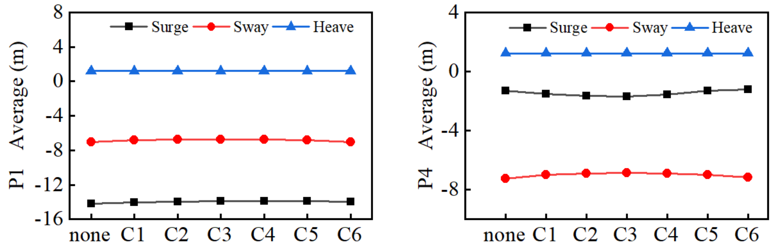

(a) Translational response

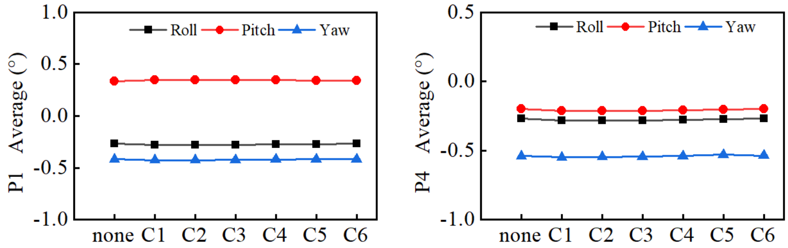

(b) Rotational response

Fig.17 Platform response at different clump weight positions

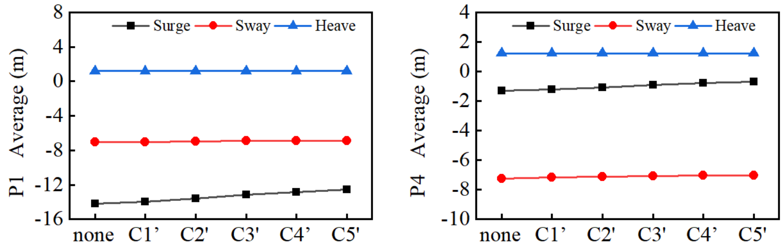

(a) Translational response

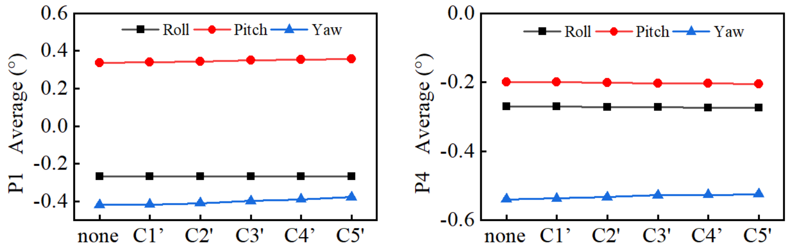

(b) Rotational response

Fig.18 Platform response with different clump weight weights

Table.7

Dynamic response of the platform with different counterweight parameters

Case	Surge/m		Sway/m		Heave/m		Roll/°		Pitch/°		Yaw/°	
	P1	P4	P1	P4	P1	P4	P1	P4	P1	P4	P1	P4
none	-14.22	-1.32	-7.09	-7.24	1.21	1.23	-0.27	-0.27	0.34	-0.20	-0.42	-0.54
C1	-14.02	-1.54	-6.86	-7.00	1.20	1.22	-0.28	-0.28	0.35	-0.21	-0.43	-0.55
C2	-13.97	-1.65	-6.78	-6.92	1.21	1.22	-0.28	-0.28	0.35	-0.21	-0.42	-0.55
C3	-13.92	-1.68	-6.74	-6.88	1.21	1.22	-0.27	-0.28	0.35	-0.21	-0.42	-0.54
C4	-13.89	-1.57	-6.76	-6.90	1.20	1.22	-0.27	-0.28	0.34	-0.21	-0.42	-0.54
C5	-13.87	-1.29	-6.85	-6.99	1.21	1.23	-0.27	-0.27	0.34	-0.20	-0.42	-0.53
C6	-13.97	-1.22	-7.03	-7.18	1.21	1.23	-0.26	-0.27	0.34	-0.20	-0.42	-0.54
C1'	-13.97	-1.22	-7.03	-7.18	1.21	1.23	-0.27	-0.27	0.34	-0.20	-0.42	-0.53
C2'	-13.61	-1.09	-6.98	-7.12	1.21	1.23	-0.27	-0.27	0.34	-0.20	-0.41	-0.53
C3'	-13.12	-0.91	-6.94	-7.07	1.21	1.23	-0.27	-0.27	0.35	-0.20	-0.40	-0.53
C4'	-12.83	-0.81	-6.92	-7.04	1.20	1.23	-0.27	-0.27	0.35	-0.20	-0.39	-0.53
C5'	-12.59	-0.71	-6.90	-7.02	1.20	1.23	-0.27	-0.27	0.36	-0.20	-0.38	-0.52

From the Fig.17 and Fig.18, it is evident that the clump weight position almost has minimal impact on the dynamic response of the platform. Increasing the weight of the clump weight results in decreased displacement in the surge and sway directions, while the other responses are not significantly affected by changes in clump weight. As can be seen in Tab. 7, surge response will be reduced by a maximum of 11.5%. However, other response The other dynamic responses are slightly influenced by the clump weight parameter, with differences ranging from 0.1. In contrast to the findings from the previous frequency domain analysis, the WM system's effect on wind farms is not significant. This is primarily due to the fact that an increase in clump weight has little impact on the platform's dynamic response at the wave frequency. Since the platform is more sensitive to wave excitation, the WM mooring system has a limited effect on the platform's overall response.

5.2.3 Buoy and clump weight mooring system

There are two types of buoys and clump weight arrangement in this wind farm, one with no buoy in the link catenary mooring (BWM) and the other with the same buoyancy buoy positioned at the middle of link catenary mooring (LBWM) as in the fixed mooring. A net buoyancy of 0.6 G and a clump weight of 5 t were chosen to investigate the dynamic response of these two arrangements on the platform's surge, sway, and yaw responses, as shown in Fig.19.

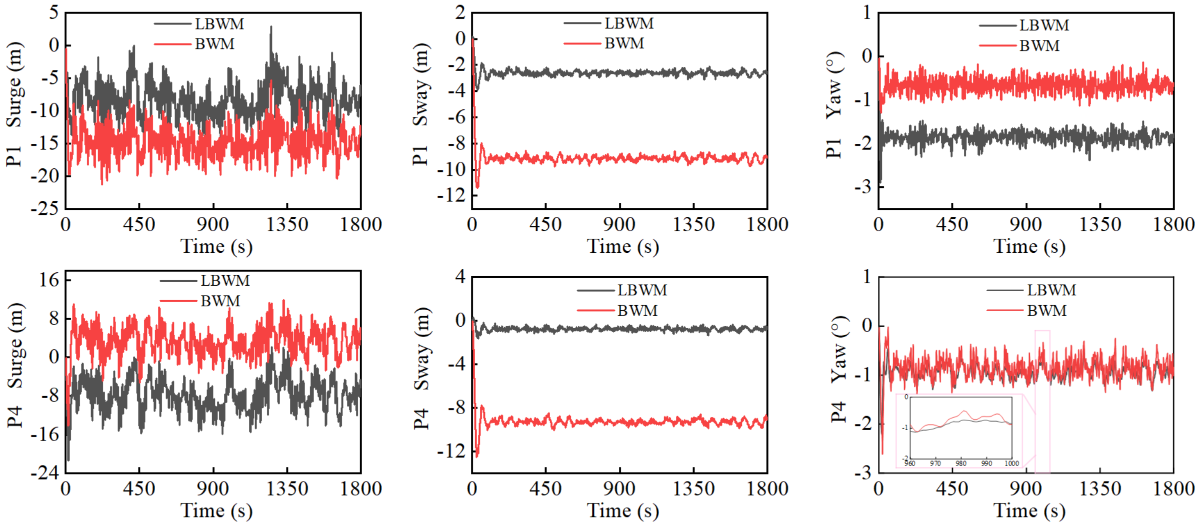

(a) Surge (b) Sway (c) Yaw

Fig.19 Dynamic response of the platform

Fig.19 illustrates that the addition of link buoys effectively reduces the sway response of each platform compared to the configuration without link buoys. This reduction can be attributed to the more uniform horizontal force exerted on the platform due to the presence of link buoys. The surge response of P1 is reduced by approximately 75% with the addition of link buoys. For P4, the addition of link buoys does not change the response amplitude but alters the direction of motion in the surge direction, causing it to drift in the direction of the wind load and follow a similar trajectory to that of P1. Due to different directions of wind and waves, P4 is more affected by waves. The link buoy weakens the wave load effect in this direction, at this time the wind load force is greater than the wave load force. Consequently, P4 is more affected by the wind load, which produces drifting motion in this direction. In terms of yaw response, the link buoys increase the mean value of P1's yaw response by approximately 50%, while the yaw response of P4 is less affected by them. The addition of link buoys reduces part of the self-weight of the mooring, resulting in a decrease in axial force in the mooring. Moreover, the yaw response is mainly influenced by the wave frequency, so the platform is prone to deflecting motion in this direction under wave load.

5.3 Analysis of mooring tension

The integrity of the mooring system plays a crucial role in ensuring the safe operation of floating wind turbines as it relies on the restoring force provided by the mooring and ballast to maintain stability. The average mooring tensions for the BM, WM and BWM mooring system were separately calculated and are presented in Fig.20, Fig.21 and Fig.22.

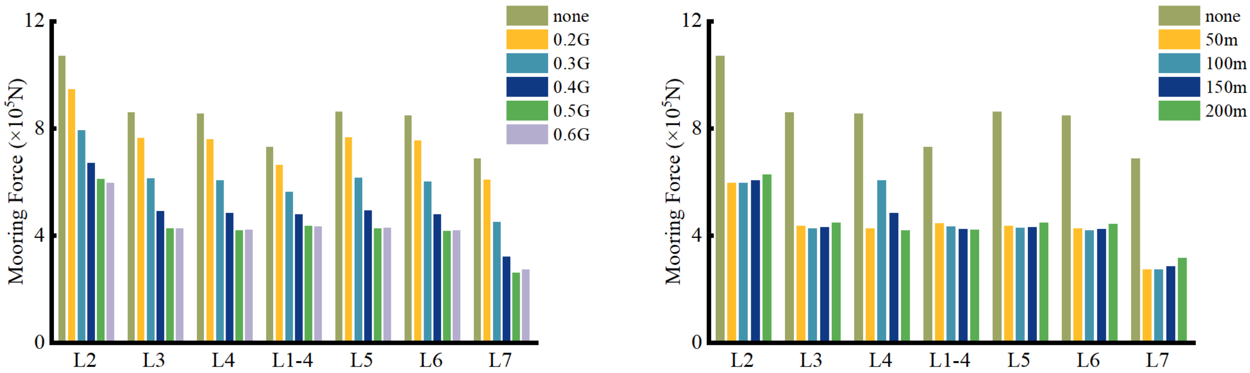

Fig.20 BM system mooring tension

From the Fig.20, it is observed that the mooring tension of L2 on the windward side of the mooring is higher than that of L7 on the leeward side in general. Regarding net buoyancy, the average mooring tension decreases as the net buoyancy of the buoys increases. Whereas, when the net buoyancy exceeds 0.5 G, the mooring tension values are less influenced by the net buoyancy of the buoys. The mooring tension is minimally affected by the position of the buoys, and there is a slight increase in tension as the distance from the fairlead increases. Nevertheless, this effect is not as significant as the impact of net buoyancy on the mooring system. Therefore, the mooring tension is primarily influenced by the net buoyancy of the buoy. On the one hand, the buoy reduces the mooring weight through net buoyancy, leading to a decrease in mooring tension. On the other hand, it reduces the platform displacement by reducing the surge and sway response, resulting in reduced mooring deformation and decreased mooring tension.

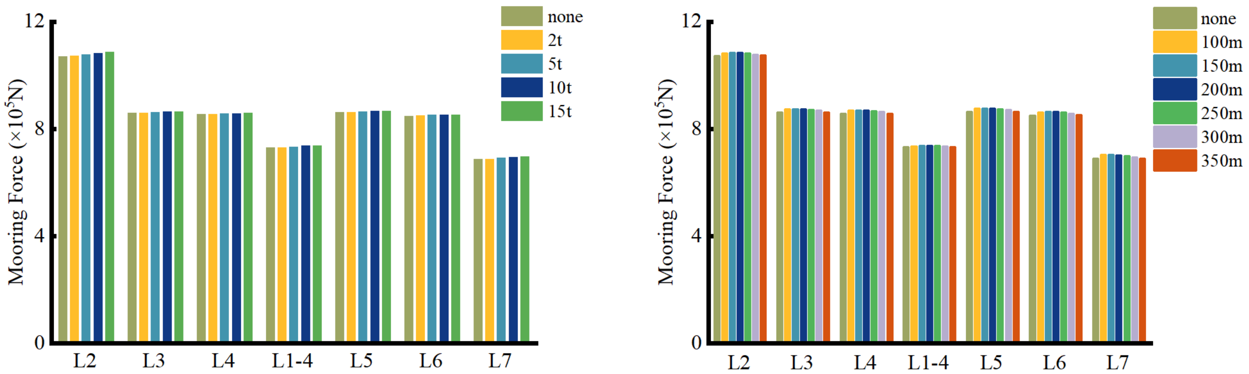

Fig.21 WM system mooring tension

From Fig.21, it can be observed that the distance of the clump weight from the fairlead has minimal impact on the average value of the mooring tension in the WM system. However, as the mass of the clump weight increases, the average mooring tension in the WM system exhibits an increasing trend. Furthermore, as the clump weight is positioned further away from the fairlead, the tension initially rises and then falls. The maximum mooring tension is reached when the clump weight is located at a distance of 200 m or 250 m from the fairlead. It can be considered that the mooring tension increases when the clump weight is situated in the middle of the mooring or has a higher weight.

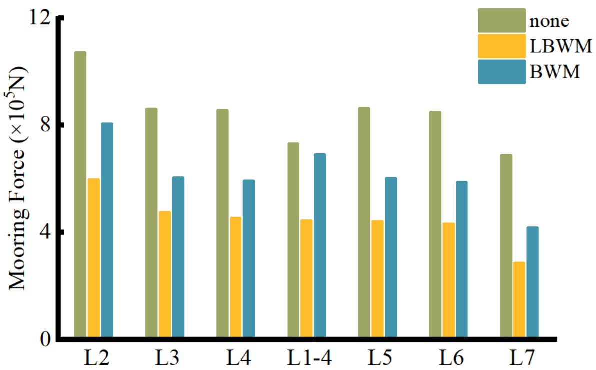

Fig.22 BWM system mooring tension

Fig.22 illustrates that the mooring tension in the wind farm experiences significant reduction with the implementation of the BWM system. Moreover, the addition of link buoys further enhances the reduction effect on mooring tension. This can be attributed to the link buoys providing a more balanced force distribution across the wind farm platform in the sway direction, thereby reducing the dynamic response in surge and minimizing platform displacement and mooring tension. The tension in the linked catenary L1~4 is reduced by 35.6% compared to the mooring without link buoys, which means that the link buoys have an effect on the mooring tension by reducing the self-weight of the mooring.

In summary, the comparison of BM, WM, and BWM systems on mooring tension in wind farms reveals that both BM and BWM systems contribute to reducing the average mooring tension, while the WM system has a comparatively lesser effect on mooring tension. The analysis of the time and frequency domain indicates that the WM system has minimal impact on the platform’s natural frequency, resulting in limited influence on surge and sway responses. The mooring tension is mainly determined by the response in the direction of surge and sway. Hence, the mooring tension does not change considerably in the WM system, but the buoys of BWM system changes the natural frequency of the platform and the response of the surge and sway, resulting in a change in mooring tension.

5.4 Analysis of the laid length

A sufficient mooring laid length is crucial to mitigate the risk of anchor pull-out caused by platform response and to provide adequate restoring force for reducing the dynamic response of the platform. However, the addition of buoys or clump weights can potentially alter the required laid length. Therefore, the laid length of the BM, WM and BWM systems is examined to prevent anchor pull-out risks resulting from insufficient laid length. The statistics of the laid length are presented in Figure 23, 24 and 25, respectively.

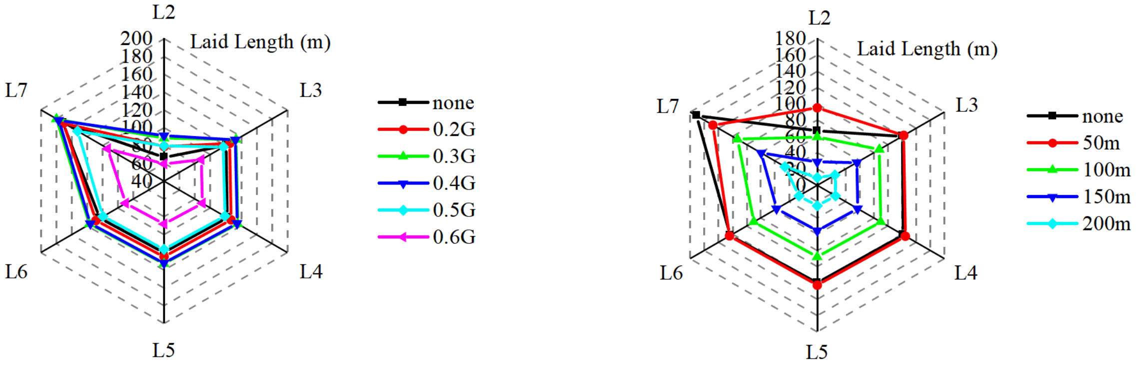

Fig.23 The mooring laid length of BM system

As revealed by Fig.23, the mean laid lengths of L3-L6 exhibit a consistent variation trend. Overall, the windward mooring L2, being more exposed to wind loads, has a shorter laid length compared to the leeward mooring L7. With the increase of buoy net buoyancy, the average value of the laid length rises and then falls. At net buoyancy of 0.3G and 0.4G, each mooring's laid length follows the same trend and reaches its maximum value. When the net buoyancy is 0.5G and 0.6G, the laid length decreases but remains within the safety margin. The buoy increases its damping, resulting in a decrease in platform displacement in the surge direction, and the laid length can be increased within a certain range. However, when the net buoyancy of the buoy becomes too large, the mooring hanging section grows, causing a corresponding decrease in the laid length. Additionally, as the distance between the buoy and the fairlead increases, the length of the mooring laid section decreases, especially when the distance exceeds 150 m, where the decrease is most significant. This is primarily due to the buoy being closer to the anchor point, resulting in a shorter laid length. Therefore, when considering the placement of buoys, it is advisable to select a position close to the fairlead.

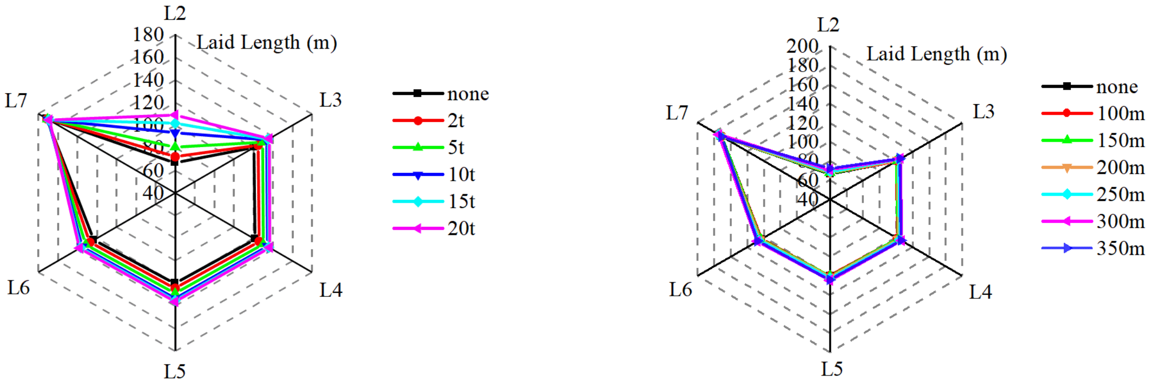

Fig.24 The mooring laid length of WM system

From Fig.24, it is obvious that the mooring laid length tends to increase as the weight of the clump weight rises, but hardly varies with the position of the clump weight. When the weight exceeds 10 t, the laid length of L3-L7 is less affected by the clump weight's weight, while the windward mooring L2 is more influenced by the clump weight's weight compared to the leeward mooring L7. Analysis of the platform's dynamic response indicates that the surge and sway responses are only slightly affected by the weight and position of the clump weight, resulting in insignificant changes in response amplitudes and mooring laid length. Moreover, considering the platform's natural frequency, the clump weight has no impact on the natural frequency of platform rotation and yaw response, and the buoy only affects the response amplitudes of surge and sway. Consequently, the length of the mooring laid length undergoes less variation compared to that of the BM system.

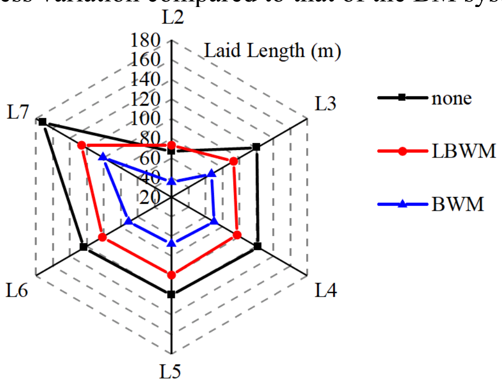

Fig.25 The mooring laid length of BWM system

Fig.25 demonstrates the notable impact of adding link buoys to the BWM system on the mooring laid length. In the absence of link buoys, the laid length of L2 is reduced by approximately 50% compared to the original wind farm mooring, significantly increasing the risk of mooring pull-out. However, with the addition of link buoys, the average laid length of L2 returns to the mean value of the original wind farm, while the other mooring lines experience a decrease in their laid lengths compared to the original configuration. The presence of the buoys reduces the self-weight of the mooring, leading to an increase the mooring overhang section and reduces the length of the laid section. The length of L7 laid section is less affected less by wind and the platform drifts under the wind load, leading to a larger surplus in laid length. Conversely, the L2 on the windward side is affected by wind and the laid length is the smallest. Therefore, it is advisable to avoid co-linearity with wind loads as far as possible when considering the mooring arrangement.

6. Conclusions

To mitigate the risk of fa tigue damage to mooring systems in floating offshore wind turbines, this study introduces the concept of a shared hybrid mooring system for implementation within floating wind farm environments. To examine the viability of the proposed system, a coupled multi-physics wind farm model is established using AQWA and FAST, considering the interactions between various physical fields. The investigation of dynamic responses of floating wind turbines under the influence of the shared hybrid mooring system yields the following conclusions:

1)The buoy mooring system reduces the natural frequency of the platform in the surge and sway directions, but increases the natural frequency and response amplitude of the platform in the roll and pitch directions. Platform 1 experiences an increase in response amplitude at the surge, sway, and heave natural frequencies, while Platform 4 shows a reduction in response amplitude at the surge natural frequency. The clump weight mooring system raises the natural frequencies in the surge and sway directions and increases the response amplitude in the yaw direction. The buoy and clump weight system exhibits similar trends in platform natural frequencies as the buoy mooring system.

2) Frequency domain analysis reveals that the buoy has a dampening effect on the surge, sway, and yaw responses of the platform. In conclusion, this paper presents a comprehensive investigation into the effects of three hybrid mooring systems on a 2×2 array wind farm using the Barge platform. Increasing net buoyancy decreases surge and sway responses, and the heave, roll, and pitch responses are more sensitive to wave frequency. The position of the clump weight has minimal impact on dynamic response, but increasing weight reduces displacement in surge and yaw directions.

3) The addition of linked buoys in the buoy and clump weight mooring system improves sway and surge responses but increases yaw response on the windward side. Mooring tension in buoy systems decreases with increased net buoyancy, while the distance between the buoy and fairlead has a slight effect. The position and weight of the clump weight have minimal influence, and the addition of link buoys reduces mooring tension. The mean length of the mooring laid section decreases with increased net buoyancy and distance between the buoy and fairlead. The weight of the clump weight affects the laid length, while position has minimal impact. The addition of link buoys increases the mooring laid length in the buoy and clump weight system.

Funding

This research was funded by the National Natural Science Foundation of China (52375193，52376204，52106262，52006148，51976131) and Acknowledges the Non-carbon energy conversion and utilization institute under the Shanghai Class IV Peak Disciplinary Development Program.

References

[1] Diesendorf, M. Scenarios for mitigating CO2 emissions from energy supply in the absence of CO2 removal. Climate Policy, 2022, 22: 882-896.

[2] IEA.Net Zero by 2050: A Roadmap for the Global Energy Sector. International Energy Agency, Abu Dhabi, 2021.

[3] Summerfield-Ryan O, Park S. The power of wind: The global wind energy industry's successes and failures. Ecological Economics, 2023, 210: 107841.

[4] Gaumond M, Rethore P E, Ott S, et al. Evaluation of the wind direction uncertainty and its impact on wake modeling at the Horns Rev offshore wind farm. Wind Energy, 2014, 17(8): 1169-1178.

[5] Lee M K, Nam J, Kim M．Valuing the public preference for offshore wind energy: The case study in South Korea. Energy, 2023, 263: 125827.

[6] Wang B, Li Y, Gao S, et al. Motion characteristics and aero-elastic responses of floating offshore wind turbine under coupling action of waves and winds. Frontiers in Environmental Science, 2022, 965334.

[7] Liu Q S, Miao W P, Li Chun, et al. Effects of trailing-edge movable flap on aerodynamic performance and noise characteristics of VAWT. Energy, 2019, 189: 116271.

[8] Wang Y B, Miao W P, Ding Q W, et al. Numerical investigations on control strategies of wake deviation for large wind turbines in an offshore wind farm. Ocean Engineering, 2019, 173: 794-801

[9] Ramachandran R C, Desmond C, Judge F, et al. Floating offshore wind turbines: Installation, operation, maintenance and decommissioning challenges and opportunities. Wind Energy Science, 2022, 7(2): 903-924.

[10] Fontana C M, Arwade S R, DeGroot D J, et al. Efficient multiline anchor systems for floating offshore wind turbines. // Proceedings of the 35th International Conference on Ocean, Offshore and Arctic Engineering, Busan: Ships and Offshore Structures, 2016.

[11] Goldschmidt, M, Muskulus, M. Coupled Mooring Systems for Floating Wind Farms. // EERA Deep Wind - 12th Deep Sea Offshore Wind R&D Conference. Trondheim: Energy Procedia, 2015.

[12] Ding Q W, Li C, Yu N T, et al. Numerical and experimental investigation into the dynamic response of a floating wind turbine spar array platform. Journal of Mechanical Science and Technology, 2018, 32(3): 1105-1116.

[13] Liu Q S, Miao W P, Yue M N, et al. Dynamic Response of Offshore Wind Turbine on 3×3 Barge Array Floating Platform under Extreme Sea Conditions. China Ocean Engineering, 2021, 35(2): 186–200.

[14] Chen Y H, Yang R Y. Study on Array Floating Platform for Wind Energy and Marine Space Optimization. Sustainability, 2021, 13: 14014.

[15] Lozon E, Hall M. Coupled loads analysis of a novel shared-mooring floating wind farm. Applied Energy, 2023, 332: 120513.

[16] Wilson S, Hall M, Housner S, et al. Linearized modeling and optimization of shared mooring systems. Ocean Engineering, 2021, 241: 110009.

[17] Liang G D, Jiang Z Y, Merz K. Dynamic analysis of a dual-spar floating offshore wind farm with shared moorings in extreme environmental conditions. Marine Structures, 2023, 90: 103441.

[18] Kwan T C T, Ma K T, Luo Y et al. Mooring system engineering for offshore structures. Cambridge: Gulf Professional Publishing, 2019.

[19] Huo F, Xu J, Yang H K, et al. Study on characteristics of mooring system of a new floating offshore wind turbine in shallow

water by experiment. Frontiers in Energy Research, 2023, 10: 1007996.

[20] Yan J, Qiao D S, Ou J P. Optimal design and hydrodynamic response analysis of deep water mooring system with submerged buoys. Ships and Offshore Structures, 2018, 13(5): 476-487.

[21] Wayman E N. Coupled Dynamics and Economic Analysis of Floating Wind Turbine Systems. Boston: Massachusetts Institute of Technology, 2006.

[22] Jonkman J, Butterfield S, Musial W, et al. Definition of a 5-MW reference wind-turbine for offshore system development. U S: U S Department of Energy Office of Scientific and Technical Information, 2009.

[23] Choi N J, Nam S H, Jeong J H, et al. Numerical study on the horizontal axis turbines arrangement in a wind farm: Effect of separation distance on the turbine aerodynamic power output. Journal of Wind Engineering & Industrial Aerodynamics, 2013, 117: 11–17.

[24] Stevens R J A, Gayme D F, Meneveau C, et al. Large eddy simulation studies of the effects of alignment and wind farm length. Journal of Renewable and Sustainable Energy, 2014, 6(2): 023105.

[25] Jonkman J, Matha D. A quantitative comparison of the responses of three floating platforms. // Presented at the European Offshore Wind 2009 Conference and Exhibition. National Renewable Energy Lab, 2010.

[26] Mavrakos S A, Chatjigeorgiou J. Dynamic behavior of deep water mooring lines with submerged buoys[J]. Computers and Structures, 1997, 64(1-4): 819-835.

[27] Ma Y, Hu Z Q, Xiao L F. Wind-wave induced dynamic response analysis for motions and mooring loads of a spar-type offshore floating wind turbine. Journal of Hydrodynamics. 2014, 26 (6): 865–874.

[28] Karimirad M X. Modeling aspects of a floating wind turbine for coupled wave–wind-induced dynamic analyses. 2013, Renewable Energy, 53: 299–305.

[29] Jeon, S H, Cho, Y U, Seo, M W, et al. Dynamic response of floating substructure of spar-type offshore wind turbine with catenary mooring cables. Ocean Engineering, 2013, 72: 356–364.

[30] Hall, M, Buckham, B, Crawford, C, Nicoll, R S. The importance of mooring line model fidelity in floating wind turbine simulations. // Oceans'11 MTS/IEEE Kona Conference. Institute of Electrical and Electronics Engineers. Hawaii, USA, 2011.

[31] Hall, M, Goupee, A. Validation of a lumped-mass mooring line model with DeepCwind semisubmersible model test data. Ocean Engineering, 2015, 104, 590–603.

[32] ANSYS. AQWA Theory Manual. Canonsburg, United States, 2013.

[33] Cummins W E, Iiuhl W, Uinm A. The impulse response function and ship motions. Schiffstechnic, 1962, 9: 124-135.

[34] Newman J N. The theory of ship motions. Advance in Applied Mechanics, 1979, 18: 221-283.

[35] Pierson W J, Moskowitz L. A Proposed Spectral Form for Fully Developed Wind Seas Based on the Similarity Theory of S. A. Kitaigorodskii. Journal of Geophysical Research, 1964, 69(24): 5181 – 5190.

[36] Moriarty P J, Hansen A C. Aero Dynamic Theory Manual. Colorado: National Renewable Energy Laboratory, 2010.

[37] Kord I. Concept Design and Analysis of Floating Wind Turbine Platforms. Ansan Korea: Korea Ocean Research and Development Institute, 2012.

[38] Mavrakos S A, Papazoglou V J, Triantafyllou M S, et al. Experimental and numerical study on the effect of buoys on deep water mooring dynamics// The First International Offshore and Polar Engineering Conference. Edinburgh: ISTP, 1991: 243-251.

[39] Jonkman B J, Kilcher L. TurbSim User's Guide. Colorado, United States, 2012.

[40] Johannessen K, Meling T S, Haver S. Joint distribution for wind and waves in the northern north sea. International Journal of Offshore and Polar Engineering, 2002, 12(1): 19-28.